nature energy

Article

https://doi.org/10.1038/s41560-022-01137-z

Redox-tunable Lewis bases for electrochemical carbon dioxide capture

Received: 25 January 2022

Accepted: 8 September 2022

Published online: 13 October 2022



Xing Li m 0 ^{1,5}, Xunhua Zhao m 0 ^{2,3,5}, Yuanyue Liu m 0 ^{2,3} $m \bowtie$, T. Alan Hatton m 0 ⁴ $m \bowtie$ and Yayuan Liu m 0 ^{1,4} $m \bowtie$

Carbon capture is considered a critical means for climate change mitigation. However, conventional wet chemical scrubbing utilizing sp^3 amines suffers from high energy consumption, corrosion and sorbent degradation, motivating the search for more efficient carbon dioxide separation strategies. Here, we demonstrate a library of redox-tunable Lewis bases with sp^2 -nitrogen centres that can reversibly capture and release carbon dioxide through an electrochemical cycle. The mechanism of the carbon capture process is elucidated via a combined experimental and computational approach. We show that the properties of these Lewis base sorbents can be fine-tuned via molecular design and electrolyte engineering. Moreover, we identify a bifunctional azopyridine base that holds promise for electrochemically mediated carbon capture, exhibiting >85% capacity utilization efficiency over cycling in a flow system under 15% carbon dioxide with 5% oxygen. This work broadens the structural scope of redox-active carbon dioxide sorbents and provides design guidelines on molecules with tunable basicity under electrochemical conditions.

The negative consequences of climate change caused by anthropogenic carbon dioxide (CO₂) emissions constitute major issues faced by our society¹. To mitigate global warming, carbon capture from point sources and directly from ambient air followed by sequestration/utilization has been broadly accepted as a critical strategy²⁻⁶. The incumbent technology for carbon capture is thermal amine scrubbing, which utilizes aqueous amine solutions for CO₂ chemisorption^{7,8}. In a typical process, strong, nucleophilic sp^3 nitrogen bases are used, where the lone-pair electrons on nitrogen act as Lewis bases to attack the electrophilic carbon of CO₂, forming carbamate adducts⁸. However, substantial thermal energy input is required to dissociate the adducts for CO₂ desorption (for example, ~110 °C for monoethanolamine regeneration)9. Moreover, amine scrubbing is challenged by complicated heat integration with existing infrastructures, thermal sorbent degradation, corrosion of process equipment and evaporative loss of toxic amines into the environment⁹⁻¹¹. Correspondingly, many new solid or liquid sorbent chemistries have been suggested, several of which have shown promising early results $^{5,6,12-14}$. Nevertheless, most of these materials still rely on complex or expensive temperature- or pressure-swing-based operations 15 . To minimize the energy consumption for carbon capture, it is critical to design sorbents with intermediate CO_2 binding energy. The interaction between sorbent and CO_2 should be sufficiently strong for effective carbon capture, but not too strong to form an overly stable adduct that is difficult to dissociate.

Here, we report a library of Lewis bases bearing redox-active sp^2 nitrogen centres whose CO_2 binding affinity can be reversibly modulated by applying electrochemical potentials. An in-depth mechanistic understanding of the reversible CO_2 complexation process is provided by combined experimental and computational evidence. We demonstrate that the redox potentials and CO_2 binding energies of these sorbents can be fine-tuned via molecular design and electrolyte engineering. Importantly, we discover that introducing different sp^2 nitrogen centres into a single molecule with extended conjugation can effectively improve the separation performance. Such a concept

¹Department of Chemical and Biomolecular Engineering, Johns Hopkins University, Baltimore, MD, USA. ²Department of Mechanical Engineering, The University of Texas at Austin, Austin, TX, USA. ³Texas Materials Institute, The University of Texas at Austin, Austin, TX, USA. ⁴Department of Chemical Engineering, Massachusetts Institute of Technology, Cambridge, MA, USA. ⁵These authors contributed equally: Xing Li, Xunhua Zhao. e-mail: yuanyue.liu@austin.utexas.edu; tahatton@mit.edu; yayuanliu@jhu.edu

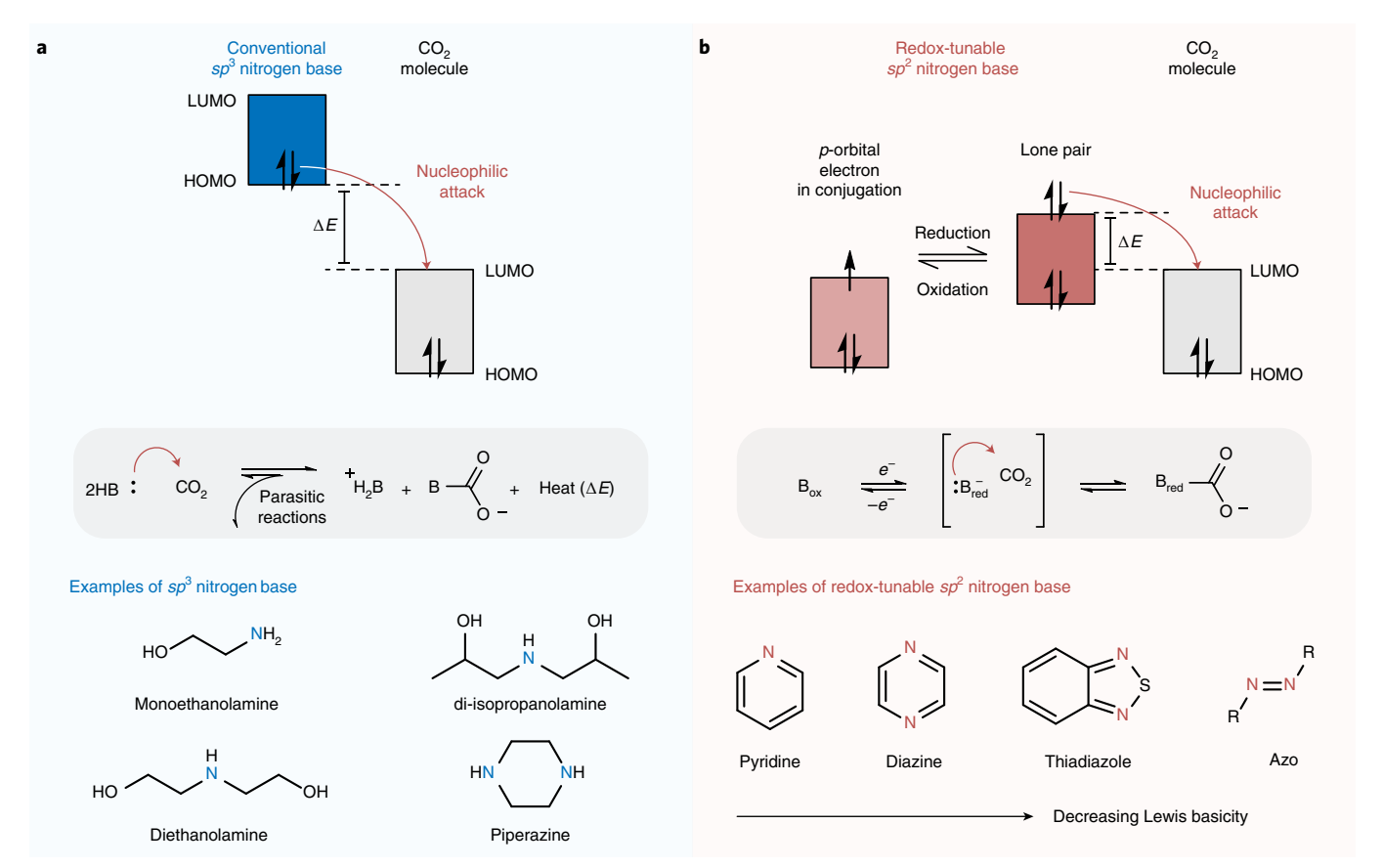


Fig. 1 | Conventional sp^3 nitrogen bases and redox-tunable sp^2 nitrogen bases for carbon capture. a,b, Energy diagrams of the sp^3 base-CO₂ adduct (a) and redox-tunable sp^2 base-CO₂ adduct (b), together with the corresponding chemical reactions and molecular examples. The red arrows

depict the nucleophilic attack of CO_2 by the lone-pair electrons from the bases. B in the chemical reaction equations stands for a base molecule, B_{ox} , oxidized base molecule; $\mathrm{B}_{\mathrm{red}}$, reduced base molecule. HOMO, highest occupied molecular orbital.

has been demonstrated successfully using 4,4'-azopyridine (AzPy) in a flow-based carbon capture system, which achieved promising capacity utilization and release/capture efficiency under simulated flue gas. This work expands the chemical space and deepens the fundamental understanding of redox-tunable CO₂ sorbents for developing electrochemically mediated carbon capture (EMCC) technologies, which have garnered considerable research attention recently $^{16-24}$. Compared with conventional methods. EMCC can operate isothermally, have the potential to desorb concentrated CO₂ at ambient or even elevated pressure and enable a modular design by not requiring substantial heat $integration {}^{22,23}. Moreover, EMCC offers exciting opportunities for more\\$ sustainable and decentralized separation processes when using electricity from renewable sources. While our demonstrated flow-based EMCC system is still limited by the relatively low ionic conductivity of ion exchange membranes in organic electrolytes and active species crossover, the discovered chemical library of redox-tunable Lewis bases can be incorporated into a plethora of solid or liquid sorbent designs in future studies to enable practical EMCC with high efficiency, selectivity and tolerance towards parasitic reactions.

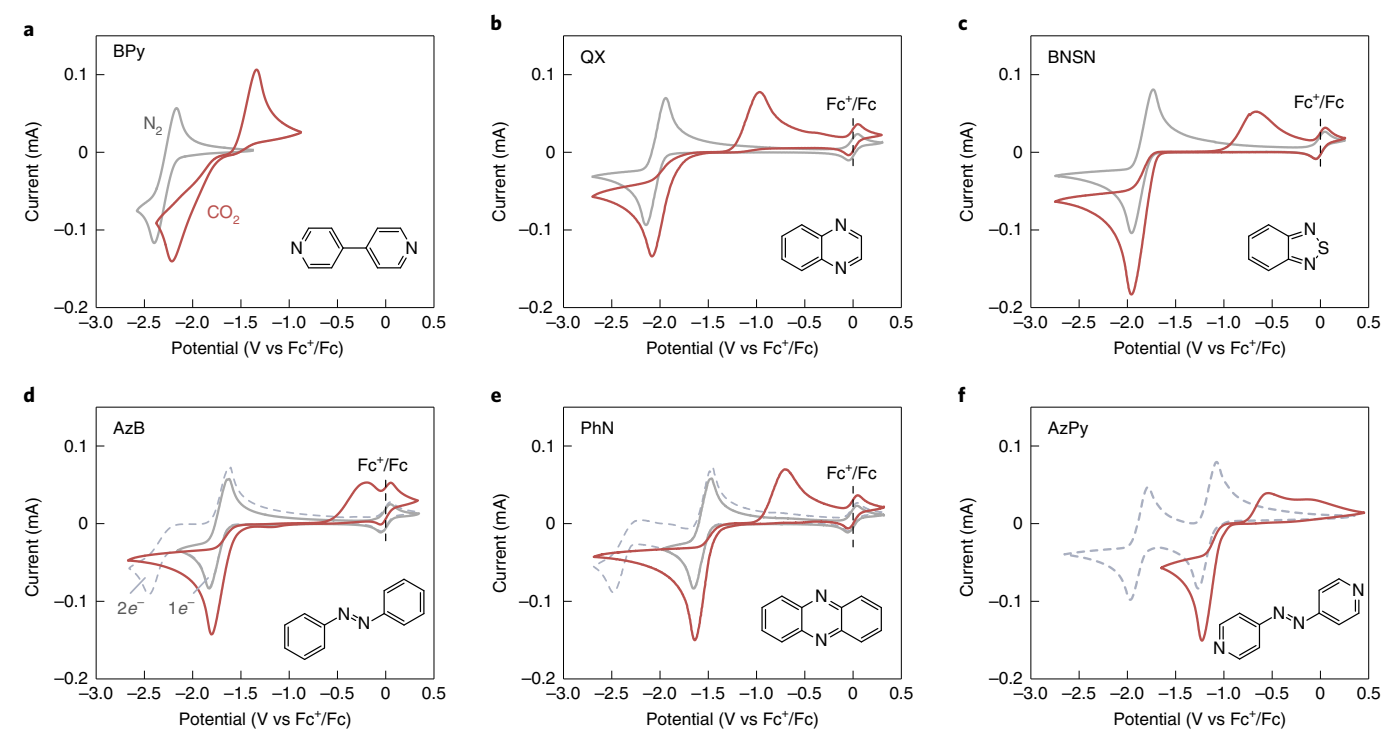
A library of redox-tunable Lewis bases for CO₂ separation

Inspired by carbamate formation in amine scrubbing using sp^3 nitrogen bases (Fig. 1a), we hypothesize that the CO_2 affinity of Lewis bases with redox-active sp^2 nitrogen centres can be modulated by electrochemical potentials to enable innovative EMCC chemistries (Fig. 1b). In their oxidized form, these organic compounds with sp^2 -hybridized nitrogen have lone-pair electrons sitting at lower energy levels than the lowest unoccupied molecular orbital (LUMO) of CO_2 and are therefore unable

to capture CO_2 . However, when being electrochemically reduced by filling one electron into the p orbital, new lone pairs are generated at a higher energy level, rendering them effective CO_2 sorbents. Subsequent electro-oxidation releases CO_2 while regenerating the sorbents.

To verify this assumption, we judiciously selected a pool of organic bases containing sp^2 nitrogen centres, including pyridine, diazine, thiadiazole and azo moieties. The representative molecules from these families of compounds discussed first are 4,4'-bipyridine (BPy), quinoxaline (QX), phenazine (PhN), 2,1,3-benzothiadiazole (BNSN), azobenzene (AzB) and AzPy. C_2 -symmetric molecules were selected to improve the specific CO_2 capacity as high symmetry in molecular design can increase the number of redox centres per molecular weight. While in the oxidized form, none of these compounds shows strong interactions with CO_2 . However, their electro-reduction and subsequent oxidation behaviour can be drastically modulated by the presence of CO_2 in the electrolyte.

Figure 2 shows the cyclic voltammograms of the aforementioned sp^2 nitrogen moieties under nitrogen (N_2) and CO_2 in an aprotic electrolyte. Under an inert N_2 atmosphere (grey curves in Fig. 2), all molecules display redox couples typical of either one-electron or stepwise two-electron transfer. The products of the first and second electron transfer are anion radicals and dianions, respectively. The half-wave potentials ($E_{1/2}$) for the first electron transfer are -2.28, -2.04, -1.85, -1.73, -1.56 and -1.19 V versus ferrocenium/ferrocene (Fc*/Fc) for BPy, QX, BNSN, AzB, PhN and AzPy, respectively. The trend of $E_{1/2}$ is relatively consistent with the basicity of the sp^2 nitrogen centres (that is, a more positive $E_{1/2}$ with a lower basicity; Supplementary Table 1), which can be explained by the fact that stronger bases are more electron rich, making it more difficult for them to accept additional electrons. Although two



 $\label{eq:fig.2} \textbf{Fig. 2} \ | \ A \ broad \ chemical space of redox-tunable \ sp^2 \ nitrogen \ bases for \ EMCC. \\ \textbf{a-f}, \ Cyclic \ voltammograms \ of \ representative \ redox-active \ Lewis \ bases \ with \ sp^2 \ nitrogen \ centres \ evaluated \ in \ this \ work \ for \ EMCC, \ including \ BPy \ (\textbf{a}), \ QX \ (\textbf{b}), \ BNSN \ (\textbf{c}), \ AzB \ (\textbf{d}), \ PhN \ (\textbf{e}) \ and \ AzPy \ (\textbf{f}) \ under \ N_2 \ (grey \ curves; \ the \ solid \ lines \ represent \ one-electron \ transfer \ and \ the \ dotted \ lines \ represent \ stepwise \ two-electron \ transfer) \ and \ CO_2 \ atmosphere \ (red \ curves). \ The \ cyclic \ voltammograms$

were collected at a scan rate of $50\,\mathrm{mV}\,\mathrm{s}^{-1}$ using $10\,\mathrm{mM}$ compound in DMSO with 0.1 M TBAPF $_6$ as the supporting salt (water < $100\,\mathrm{ppm}\,\mathrm{by}$ Karl Fischer titration). Glassy carbon (3 mm), platinum wire and silver wire were used as the working, counter and reference electrodes, respectively. Ferrocene was used as an internal reference.

redox centres exist in BPy, QX and BNSN, only one electron transfer can be observed in the cyclic voltammogram due to the limited electrochemical stability window of the electrolyte.

Cyclic voltammograms collected under CO_2 (red curves in Fig. 2) show an anodically shifted reduction potential with a pronounced increase in peak current for all molecules. Specifically, the reduction peak is doubled compared with the first electron transfer under N_2 , indicating that the two electrons can be transferred at nearly the same potential in the presence of CO_2 . The results clearly suggest the existence of chemical interactions between reduced nitrogen centres and CO_2 . Furthermore, the oxidation peaks are also positively shifted and become quasi-reversible, which is consistent with CO_2 adduct formation that requires an extra energy input to break the nitrogen–carbon bonds.

Notably, the electrochemical behaviour of the redox-active sp^2 nitrogen moieties demonstrates a solid resemblance to that of quinones previously investigated for EMCC²⁵⁻²⁸. Supplementary Fig. 1a shows the cyclic voltammograms of 9,10-anthraquinone-a representative quinonoid molecule known for reversible CO₂ complexation. Under N₂, the electro-reduction of 9,10-anthraguinone follows the typical stepwise two-electron transfer process, and the two reduction peaks correspond to the formation of the semiquinone radical and quinone dianion²¹⁻²³. However, only one broadened reduction peak with increased current is observed under CO₂, which is attributed to the complexation between reduced quinone and CO₂ following an ECEC mechanism (where E represents electron transfer and C represents chemical reaction), as shown in Supplementary Fig. 1b. Nevertheless, in-depth mechanistic understanding of the observed electrochemical behaviour remains lacking. We hypothesize that the interaction between CO_2 and the redox-active sp^2 nitrogen centres shown in Fig. 2 also follows the ECEC mechanism, which can capture and release CO₂ through reversible carbamate formation.

Distinct from amine scrubbing, which requires two equivalents of amine to react with one equivalent of CO_2 , sp^2 nitrogen compounds can capture CO_2 stoichiometrically to their redox centres, promising high specific capacities and energy efficiencies for CO_2 removal. These chemistries broaden the design space for EMCC involving redox-active organic sorbents, which rarely exceeded the commonly available quinone molecules (except for a few reports on pyridine and disulfide) 29,30 .

CO₂ separation mechanism with redox-tunable Lewis bases

To gain fundamental insight into the mechanism of CO_2 separation with redox-tunable Lewis bases, we conducted density functional theory (DFT) calculations to interrogate the thermodynamics of the process 31 . Calculation details are reported in Supplementary Note 1, Supplementary Fig. 2 and Supplementary Table 2. We consider seven elementary steps following an ECEC mechanism. The process is illustrated in Fig. 3 using QX as an example, and each step is described in the corresponding caption. We calculated the potentials and CO_2 binding energies for the redox and CO_2 complexation/dissociation steps, respectively. Other paths have been checked but found not to be plausible. For example, neither the first CO_2 complexation before the first electron transfer nor the second CO_2 complexation before the second electron transfer is stable in DFT relaxation.

The DFT results summarized in Table 1 are consistent with the experimental data. For step 1, excellent agreement was observed between the calculated potentials and the experimental $E_{1/2}$ under N_2 , supporting the accuracy of the DFT method. After one-electron reduction, the sp^2 nitrogen moieties show a negative CO_2 binding energy in step 2, indicating that the carbamate formation reaction is thermodynamically favourable. Notably, a linear correlation exists between the reduction potential in step 1 and the CO_2 binding

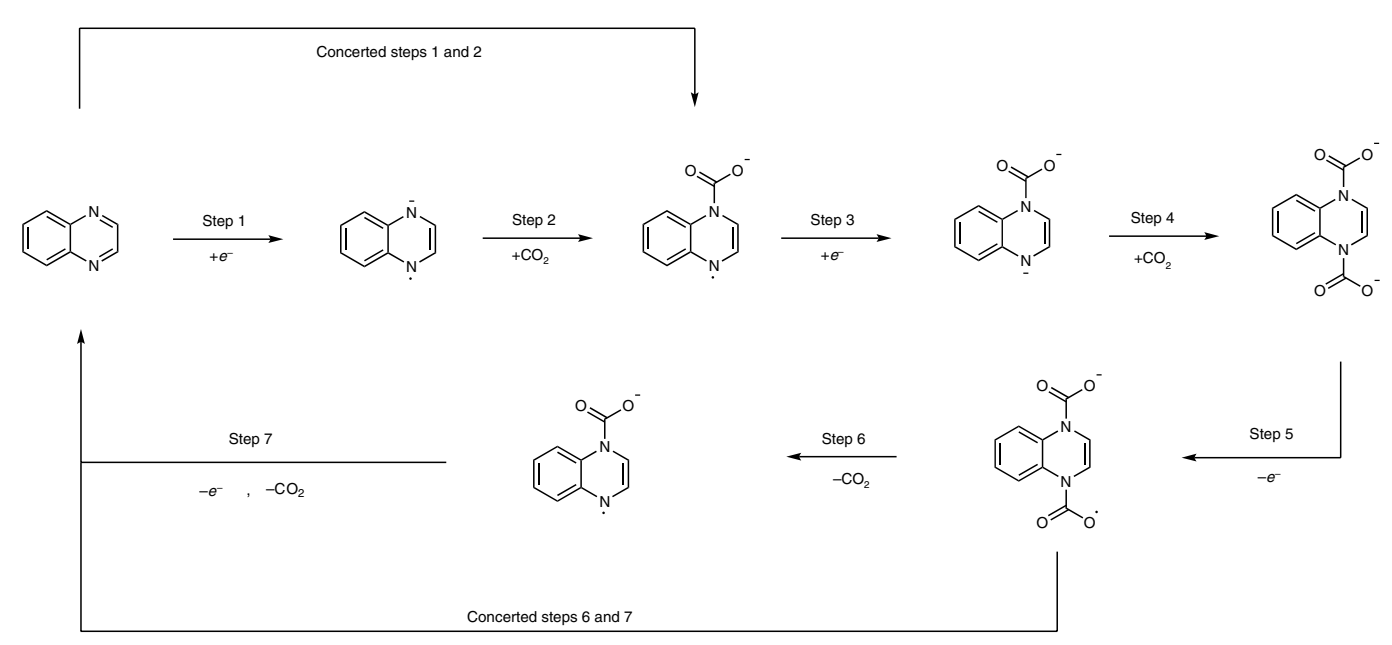


Fig. 3 | The seven elementary reaction steps (ECEC mechanism) considered in the DFT calculations. The process is illustrated using QX as an example, which sequentially involves: (step 1) sorbent reduction by one-electron transfer; (step 2) complexation with one CO, molecule; (step 3) further reduction of the

 $sorbent-CO_2\ adduct\ by\ another\ electron\ transfer; (step\ 4)\ complexation\ with\ another\ CO_2\ molecule; (step\ 5)\ oxidation\ of\ the\ adduct\ by\ one-electron\ transfer; (step\ 6)\ dissociation\ of\ one\ CO_2\ molecule; and\ (step\ 7)\ further\ adduct\ oxidation\ by\ another\ electron\ transfer\ and\ CO_2\ dissociation.$

energy in step 2 (Supplementary Fig. 3). This is consistent with the potential-basicity trend discussed above and may provide an easy way to qualitatively compare CO_2 binding energies for the future screening of redox-tunable sorbents.

The experimental observation of a positively shifted reduction potential under CO_2 compared with the first electron transfer step under N_2 (Fig. 2; particularly pronounced for BPy and QX) made us wonder whether steps 1 and 2 occur strictly in a sequential manner. Therefore, we also considered the likelihood of a concerted pathway where sorbent reduction and CO_2 complexation occur simultaneously (concerted steps 1 and 2 in Fig. 3). The calculated potentials for the concerted reaction are approximately 150–800 mV more positive than those for step 1 alone, underlining the possibility of a concerted pathway. Nevertheless, the reaction mechanism can vary between redox systems and depend on the concentration of the reactants. Thus, the actual scenario is probably a combination of the stepwise and concerted pathways.

Another fundamental electrochemical behaviour we aim to explain via DFT is the anodically shifted reduction potential for the second electron transfer under CO₂. Table 1 compares the calculated second reduction potentials with (step 3) and without (the rightmost two columns) carbamate formation. Consistent with the cyclic voltammograms, the second reduction potentials are much more negative than the first (step 1) without CO₂. However, the potential for step 3 becomes very close to or even slightly more positive than that for step 1 after the CO₂ complexation reaction in step 2. This is due to the electrophilic nature of CO₂ that withdraws the electron density away from the one-electron-reduced sorbent molecules, giving rise to a decreased LUMO level that is more favourable for the second electron transfer (Supplementary Fig. 4). In subsequent step 4, another CO₂ molecule can be added to the fully reduced sorbents with a higher binding energy than in step 2. Supplementary Fig. 5 shows the DFT-optimized conformations of the adducts. Since AzPy has two types of nitrogen centre, CO₂ complexations with both the azo and the pyridine moieties were considered (Supplementary Fig. 6). Judging from the calculated reduction potentials (step 3), CO₂ complexation is likely to occur at the azo nitrogens, and a more detailed discussion on AzPy is provided in the section 'Mechanistic investigation of AzPy'.

Since CO_2 complexation creates an energy barrier to sorbent regeneration, we further evaluated the oxidation potentials for CO_2 release. Interestingly, the calculated potentials for step 5 are more positive than for step 7 for all of the molecules assessed here. Therefore, step 5 dictates the potential for CO_2 release. Once the potential for step 5 is reached, the reaction can proceed spontaneously to release two CO_2 molecules per sorbent molecule (concerted steps 6 and 7 in Fig. 3). The calculated values for step 5 are also consistent with experimentally measured onset potentials for adduct oxidation.

Our DFT calculations successfully explain the various electrochemical features observed in cyclic voltammetry to elucidate the mechanism for carbon capture and release. These have not been systematically discussed previously in EMCC using redox-active organic compounds. PhN and azo compounds possess desirable, relatively intermediate CO_2 binding energies among the sp^2 nitrogen moieties. The numbers are -0.228, -0.143 and 0.094 eV for PhN, AzB and AzPy in step 2 and -0.803, -1.137 and -0.822 eV in step 4, respectively. In comparison, the heats of reaction between conventional sp^3 amines and CO_2 are typically in the range of 0.80-1.35 eV^{14,15}. The weaker interaction between CO_2 and the redox-tunable Lewis bases is further confirmed by the longer N–C_{carbon dioxide} bond lengths (Supplementary Table 3). Since the energy required to break the N–C bond during sorbent regeneration scales proportionately with the CO_2 binding energy, PhN and azo compounds are particularly favourable for designing energy-efficient EMCC processes.

Sorbent tuning via molecular and electrolyte designs

With the library of redox-tunable Lewis bases identified and a deeper understanding of the reaction mechanism, we now aim to design sorbents with desirable properties for practical EMCC. Specifically, they should have a relatively positive reduction potential for reduced sensitivity towards molecular oxygen (O_2) —a common impurity in gas streams. Moreover, a small voltage gap between reduction and oxidation is desirable to minimize the separation energy consumption, which is dictated by the CO_2 binding energy. The immense structural diversity of organic molecules makes it feasible to tune their properties via molecular engineering.

A₇Pv⁶

-1.189

	Reduction and CO ₂ capture							Oxidation and CO_2 release				For comparison		
	Step 1 (V versus Fc+/Fc)		Step 2 (eV)	Concerted steps 1 and 2 (V)		Step 3 (V)	Step 4 (eV)	Step 5 (V)	Step 6 (eV)	Step 7 (V)		Second e transfer (ond electron sfer (V)	
		Exp. ^a	_	Exp. ^b		_					Exp. ^b		Exp. ^a	
ВРу	-2.232	-2.282	-0.717	-1.516	-1.670	-2.295	-1.099	-1.521	0.325	-1.516	-1.563	-3.146	_c	
QX	-2.055	-2.042	-0.512	-1.543	-1.548	-2.153	-1.181	-1.003	-0.031	-1.543	-1.233	-3.330	_c	
BNSN	-1.771	-1.845	-0.432	-1.340	-1.691	-1.980	-1.018	-0.819	-0.143	-1.340	-0.967	-3.057	-3.062	
AzB	-1.670	-1.730	-0.143	-1.527	-1.520	-1.627	-1.137	-0.256	-0.233	-1.527	-0.553	-2.711	-2.350	
PhN	-1.572	-1.559	-0.228	-1.344	-1.410	-1.793	-0.803	-0.847	-0.143	-1.344	-0.962	-2.644	-2.345	
AzPy ^d	-1.110	-1.189	0.094	-1.203	-0.933	-1.082	-0.822	-0.188	-0.448	-1.203	-0.767	-2.113	-1.895	

Table 1 | Summary of the DFT calculation results, including comparisons with the experimental data

"Experimental half-wave potential ($E_{1/2}$) obtained under N_2 . Experimental onset potential for reduction or oxidation obtained under CO_2 . Not measurable due to the limited stability window of the DMSO-based electrolyte. Based on the formation of azo adduct. Based on the formation of pyridine adduct.

The oxidation of reduced sorbents by O₂ is one potential source of inefficiency in our described EMCC scheme. Ideal sorbents have a reduction potential more positive than approximately -1.2 V versus Fc⁺/Fc, which is the formal potential for oxygen reduction (O_2/O_2^{-}) in aprotic electrolytes³². Introducing electron-withdrawing groups (EWGs) to the molecular structure will pull the electron density away from the sp² nitrogen lone pairs, thus shifting the reduction potential anodically. Figure 4a-c and Supplementary Fig. 7 show cyclic voltammograms of various derivatized sp² nitrogen moieties (molecular structures are provided in Supplementary Fig. 8), with the corresponding onset potentials for carbon capture and release summarized in Fig. 4d. As expected, the extra benzo group in PhN compared with QX efficiently delocalizes the electron density in the diazine ring, leading to an approximately 0.5 V increase in the reduction potential. EWGs such as trifluoromethyl (CF₃), cyano (CN) and nitro (NO₂) can also increase redox potentials, with shifts positively correlated with their Hammett constants. For example, adding two CF₃ groups to PhN further increases the reduction potential by approximately 400 mV.

-0.378

-0.732

Importantly, since the strength of interaction between CO_2 and reduced sorbents is proportional to the local electron density at the nitrogen centre, EWGs can also reduce the CO_2 binding energy. Therefore, it is possible to optimize sorbents with both a high reduction potential for O_2 stability and an intermediate CO_2 binding energy for low separation energy consumption. Figure 4d visualizes the voltage gap between sorbent reduction and adduct oxidation, which is a good indicator for the CO_2 binding energy. We indeed observed a general trend of reduced binding energy with stronger EWGs. However, as CO_2 complexation requires sufficiently nucleophilic binding sites, adduct formation will not occur if the EWGs are too strong. For example, when a strongly electron-withdrawing nitro group was introduced to a relatively weak base of BNSN, the electrochemical behaviour under CO_2 became identical to that under N_2 (Fig. 4c). The effects of EWGs are further corroborated by DFT calculations (Supplementary Table 4).

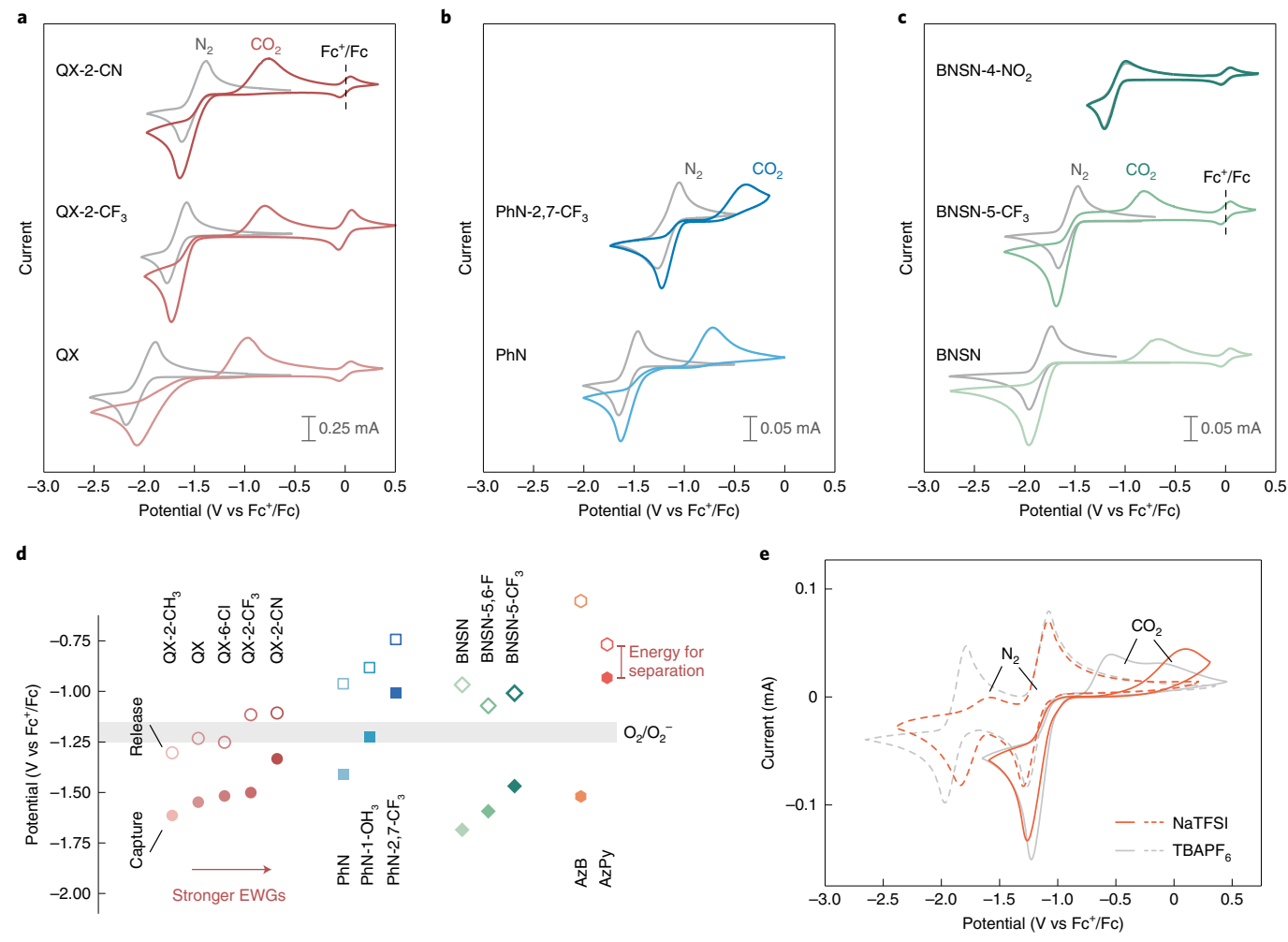
Besides EWGs, we discovered that sorbent properties can be uniquely improved by constructing multifunctional Lewis bases, where the molecular scaffold possesses different sp^2 nitrogen centres in extended conjugation. For example, by covalently soldering the most CO_2 -affinitive pyridine and the easy-to-reduce azo into a conjugated molecule, AzPy displays a superior EMCC behaviour with a high onset reduction potential of -0.93 V versus Fc^+/Fc and a narrow voltage gap of approximately 170 mV when using 0.1 M tetrabutylammonium hexafluorophosphate (TBAPF $_6$) in dimethyl sulfoxide (DMSO) as the electrolyte, corresponding to a theoretical energy consumption of 16 kJ mol $^{-1}$ CO_2 . The mechanistic cause for such a unique behaviour will be discussed in the section 'Mechanistic investigation of AzPy'.

The electrolyte environment also modulates the sorbent behaviour. Compared with the bulky tetrabutylammonium cation (TBA $^+$) with a low tendency for anion association, smaller cations can coordinate more strongly with the negatively charged sorbent– CO_2 adducts to improve their stability against O_2 (Fig. 4e and Supplementary Fig. 9). For AzPy, the adduct oxidation potential in the presence of Na $^+$ was increased by approximately 300 mV compared with that with TBA $^+$ (Fig. 4e), which became appreciably higher than the formal potential of O_2/O_2 . Divalent cations interact even more strongly with CO_2 adducts through Coulombic interactions. For example, the AzPy– CO_2 adducts precipitated in the presence of Zn $^{2+}$ and the solids were found to have a high O_2 tolerance.

Mechanistic investigation of AzPy

We believe that incorporating pyridine and azo functionalities in a conjugated manner in AzPy can stabilize the reduced molecule via resonance (Supplementary Fig. 10a) to shift the reduction potential anodically. To verify this hypothesis, we compared AzPy with 2,2'-azopyridine (2,2'-AzPy), which also possesses four sp^2 nitrogen centres, but the conjugation is partially broken (Supplementary Fig. 10b). As a result, 2.2'-AzPv cannot resonate into other forms when reduced, leading to a more negative reduction potential (Supplementary Fig. 10c). Importantly, unlike introducing EWGs where both the reduction and the oxidation potentials tend to shift anodically together, AzPy displays a significantly more positive reduction potential compared with AzB, yet the oxidation potential is even lower than that of AzB (Fig. 4d). This is probably because EWGs usually lower the energy levels of both the LUMO and the highest occupied molecular orbital (HOMO), while the bifunctionality strategy promotes CO₂ dissociation by forming the conjugated structure.

Competition might exist between the pyridine and azo moieties in AzPy for CO $_2$ complexation. Therefore, we investigated the carbamate formation mechanism via Fourier-transform infrared spectroscopy (FTIR) (Supplementary Fig. 11). AzPy exhibits three characteristic FTIR bands at 1,584, 1,566 and 839 cm $^{-1}$, which are assigned to C–N $_{\rm azo}$ stretching, C–N $_{\rm pyridine}$ stretching and C–H out-of-plane bending from the pyridine ring 33 . After the complete electro-reduction of AzPy under CO $_2$, carbamate formation is confirmed by the appearance of a C=O stretching band at 1,605 cm $^{-1}$. FTIR spectra also reveal that the azo group is more likely to be the CO $_2$ binding centre. If pyridine were the CO $_2$ binding centre, the azine resonance form would dominate such that the C–N $_{\rm azo}$ stretching band should vanish. Nevertheless, this characteristic band remains after reduction with a red shift, consistent with the fact that electro-reduction increases the electron density of AzPy. Furthermore, the C–N $_{\rm azo}$ stretching exhibits a smaller red shift



 $\label{eq:constraints} \textbf{Fig. 4} \ | \ Molecular \ and \ electrolyte \ engineering \ concepts \ to \ optimize \ the \ CO_2 \ separation \ performance \ of \ redox-tunable \ Lewis \ base \ sorbents. \ a-c, \ Cyclic \ voltammograms \ of \ derivatized \ QX \ (a), \ PhN \ (b) \ and \ BNSN \ (c). \ Supplementary \ Fig. 8 \ shows \ the full \ names \ and \ corresponding \ molecular \ structures \ of \ the \ abbreviated \ molecules. \ d, \ Summary \ of \ the \ onset \ potentials \ for \ CO_2 \ capture \ (filled \ symbols) \ and \ release \ (open \ symbols) \ of \ the \ various \ sorbent \ molecules$

tested in **a**-**c** and Supplementary Fig. 7. The molecules in each family are arranged with increasing EWG strength from left to right. The shaded region corresponds to the formal potential of the oxygen reduction in aprotic electrolytes. **e**, Cyclic voltammograms of AzPy with either TBAPF₆ (grey curves) or NaTFSI (orange curves) as the supporting salt.

than the C–H out-of-plane bending since carbamate formation on the azo group draws the electron density away. Besides, DFT calculations were conducted to predict the FTIR vibrational bands of the azo and pyridine adducts (Supplementary Tables 5–7). The simulated results of the azo adduct show much better agreement with the experimental observation. The colour change of AzPy during electro-reduction (Supplementary Fig. 12) further supports the formation of the azo adduct, and a discussion is included in Supplementary Note 2.

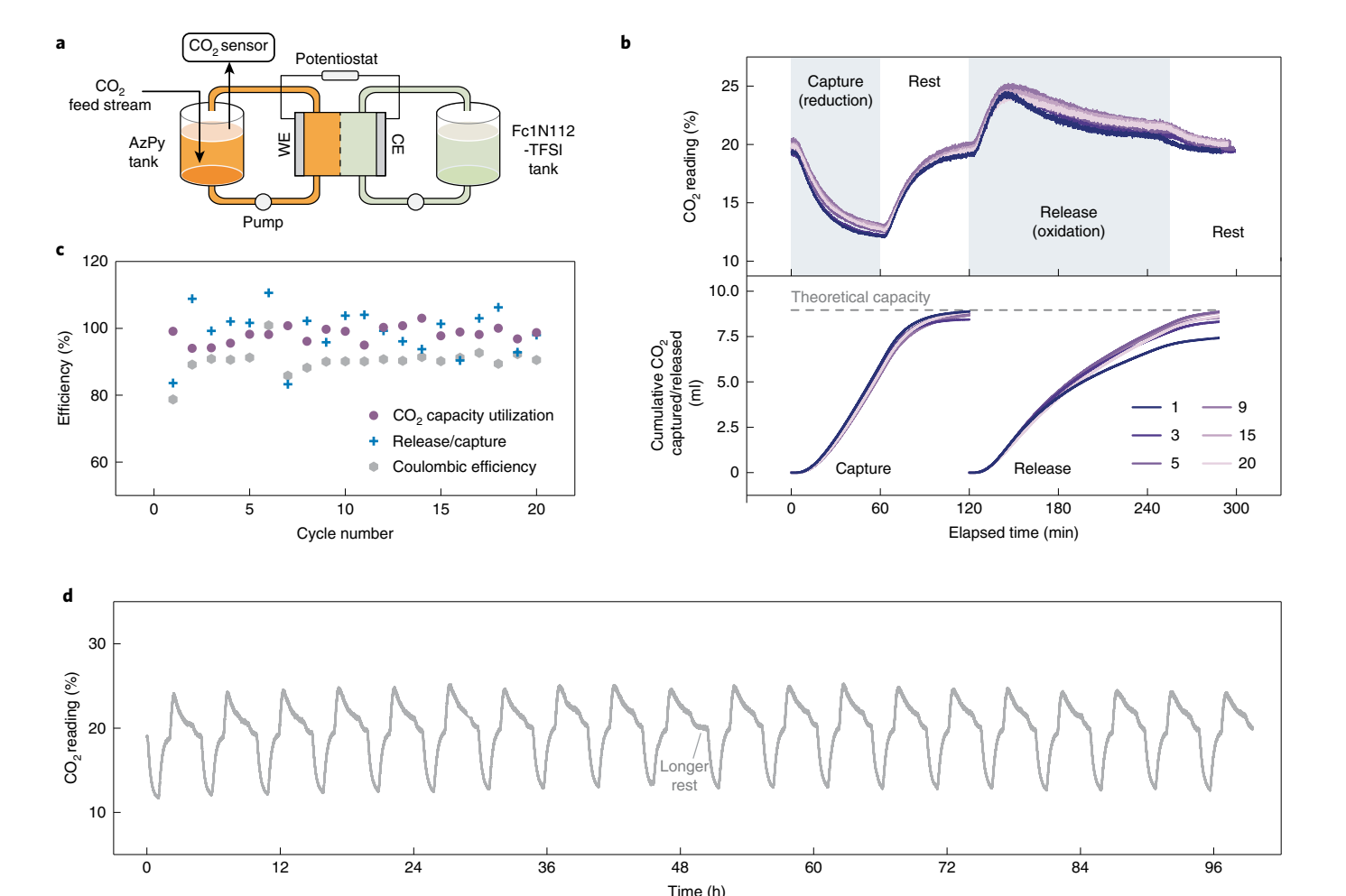
The calculated CO_2 binding constant and the reaction rate constant of AzPy are reported in Supplementary Note 3 using data shown in Supplementary Fig. 13.

Separation flow cells with redox-tunable Lewis bases

Our reported families of redox-tunable Lewis bases provide a versatile toolbox for designing functional EMCC materials, which can be either immobilized on electrodes as adsorbents or dissolved in electrolytes for continuous-flow carbon capture. Herein, we constructed a flow EMCC device (Fig. 5a and Supplementary Fig. 14) to evaluate the intrinsic performance of redox-tunable sp^2 nitrogen bases via cyclic capture-release operations.

The system was composed of a sorbent tank and a counter electrolyte tank for charge balancing. We chose a derivatized ferrocene (ferrocenylmethyl dimethyl ethyl ammonium bis(trifluoromethanesulfonyl) imide (Fc1N112-TFSI)) as the active species for the counter electrolyte due to its high solubility and electrochemical reversibility (Supplementary Fig. 15)34,35. Liquids in the two tanks were circulated through an electrochemical flow cell with carbon electrodes separated by a Nafion membrane. During operation, the sorbents undergo reduction, CO₂ exposure, oxidation and CO₂ release in a cyclic manner. A CO₂ feed stream was bubbled into the sorbent tank at a fixed flow rate and the concentration at the gas exit was measured using an online sensor to quantify the capture/release behaviour. A high active material solubility is desirable when formulating liquid sorbents (Supplementary Table 8). The best-performing AzPy has a solubility of 0.59 M in 0.5 M lithium bis(trifluoromethylsulfonyl)imide (LiTFSI) DMSO solution at 293.5 K (1.18 M theoretical CO₂ capacity, competitive with the working capacities of traditional amines)10. Further improvement can be achieved through molecular engineering²³.

Using AzPy as an example (20% CO_2 feed gas), the exiting CO_2 concentration from the sorbent tank and the corresponding system efficiencies are shown in Fig. 5b–d. Figure 5b overlays the CO_2 reading

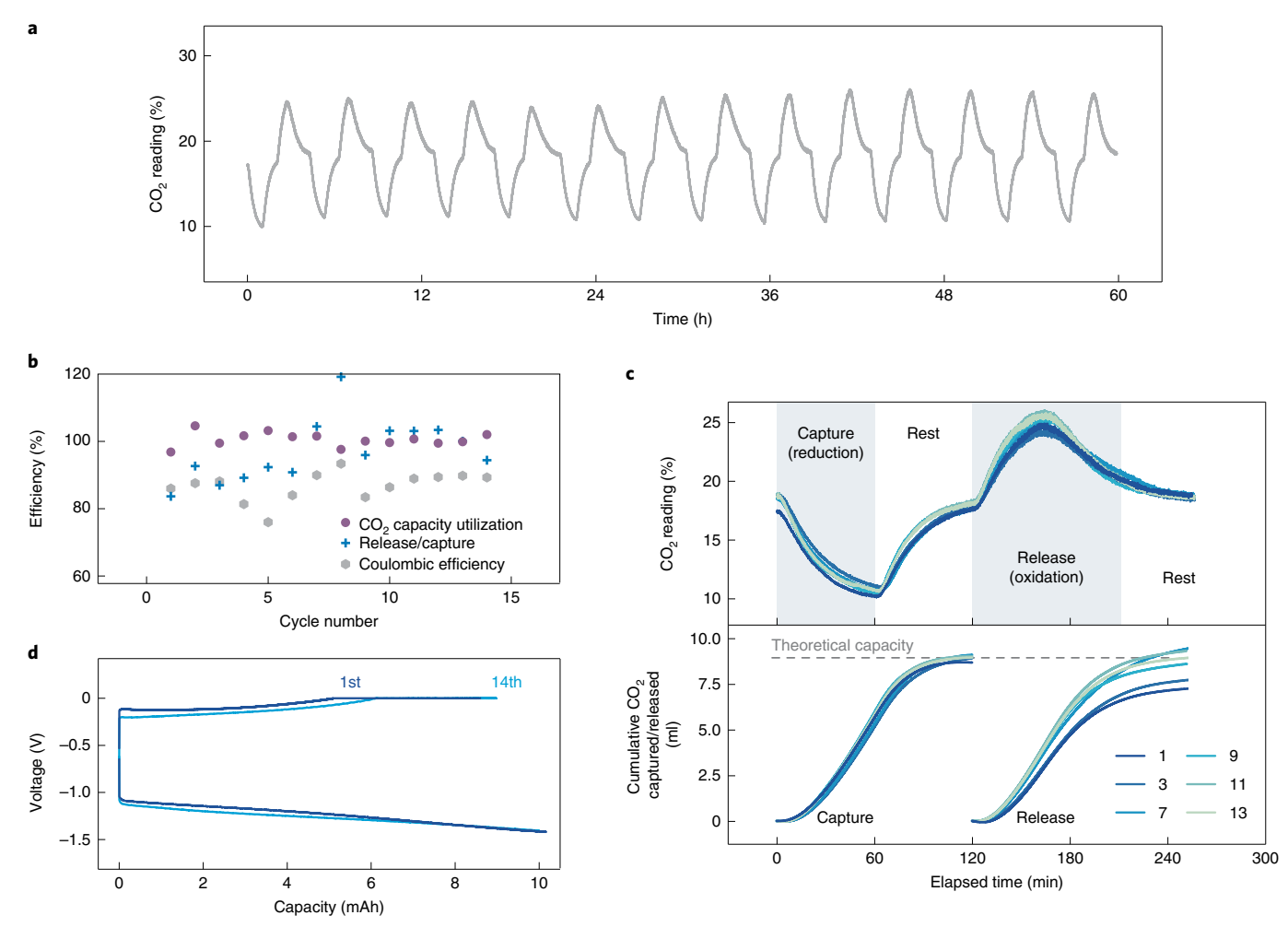


 $\label{eq:Fig.5} Fig. 5 | CO_2 separation performance in an EMCC flow cell with AzPy. a, Schematic of the flow separation system. The AzPy tank was filled with plastic beads and continuously bubbled with <math>20\%\,CO_2$ at a flow rate of 2 standard cubic centimetres per minute (sccm). The liquid sorbent was composed of 5 ml $0.2\,M$ AzPy dissolved in diethylene glycol dimethyl ether with $0.5\,M$ NaTFSI as the supporting salt. On the opposite side, an Fc1N112-TFSI tank was used to balance the charge, which was filled with $10\,ml\,0.1\,M$ Fc1N112-TFSI with $0.5\,M$ NaTFSI as the supporting salt. Both liquids were circulated through an electrochemical cell (5 cm² electrode area) at a liquid flow rate of $3\,ml\,min^{-1}$. CE, counter electrode; WE, working electrode. **b**, Top, CO_2 readings for selected capture-release

cycles. Bottom, cumulative amounts of CO_2 captured and released in each cycle relative to the theoretical capacity. Lighter colours represent later cycles. The capture, rest, release and rest steps are indicated by the shaded regions. For CO_2 capture, AzPy was reduced at 10 mA for 1 h followed by a 1-h rest. For CO_2 release, the adducts were oxidized at 10 mA to 0 mV followed by a 2-h constant voltage hold, and finally rested for another 45 min. \mathbf{c} , CO_2 capacity utilization efficiency (purple circles), release/capture efficiency (blue crosses) and Coulombic efficiency (grey hexagons) of the system for 20 capture–release cycles. \mathbf{d} , CO_2 readings at the exit of the AzPy tank over repeated capture and release cycles for -100 h of operation.

curves of selected cycles, and integrating these curves quantifies the cumulative CO₂ captured/released. For each cycle, AzPy was first reduced for 1 h, during which the drop in the exiting CO₂ concentration confirmed carbon capture. The current was then switched off for 1 h, during which the CO₂ reading gradually returned to the baseline as the remaining reduced AzPy reacted with CO₂ and the headspace was completely exchanged23. Subsequently, the AzPy-CO2 adduct was oxidized following a constant current/constant voltage oxidation protocol (details are described in the caption of Fig. 5 and the Methods), where a CO₂ desorption spike was detected. The current was then switched off to fully release the CO₂ oversaturated in the electrolyte. Consistent gas responses were observed for these 20 cycles (Fig. 5d). Note that the rests between capture and release are unnecessary for actual practice but were adopted here to allow the CO₂ reading to return to the baseline. Only by doing so can we accurately determine the amount of CO₂ captured/released by the sorbent through integrating the gas response curves. Otherwise, it is difficult to separate the capacity contribution from the physical solubility of CO₂ in the electrolyte under different headspace CO₂ concentrations.

We define the CO₂ capacity utilization efficiency as the amount of CO₂ captured relative to the theoretical value (one CO₂ molecule per electron), the release/capture efficiency as the amount of CO₂ released relative to the amount captured, and the Coulombic efficiency as the electrochemical sorbent oxidation capacity relative to the reduction capacity. In Fig. 5c, the first-cycle CO₂ capacity utilization efficiency is close to 100%, suggesting fast reaction kinetics and high selectivity of AzPy for CO₂ capture. The capacity utilization efficiency of AzPy is appreciably higher than that reported in our recent flow EMCC system with quinone chemistry, which only has a value of ~70% under similar testing conditions²³. Moreover, the capacity utilization efficiency exhibits negligible decay within the error of quantification over 20 cycles, indicating the stability and reversibility of the sorbent, which is further supported by the release/capture efficiency hovering around 100%. The Coulombic efficiency of the system is ~90%. The inefficiency is caused by the fact that adduct oxidation is not set to proceed completely under our constant current/constant voltage protocol. An extended constant voltage hold period between cycles would probably improve the Coulombic efficiency. Another source of inefficiency is



of CO $_2$ captured and released in each cycle relative to the theoretical capacity. Lighter colours represent later cycles. The capture, rest, release and rest steps are indicated by the shaded regions. For CO $_2$ capture, AzPy was reduced at 10 mA for 1 h followed by a 1-h rest. For CO $_2$ release, the adducts were oxidized at 10 mA to 0 mV followed by a 1-h constant voltage hold, and finally rested for another 45 min. **d**, Corresponding voltage–capacity curves for the first and fourteenth capture–release cycles. We noticed that the infrared-based sensors showed a slight baseline drift in the presence of O $_2$ that could impact the integration of the cumulative capture/release amount, making the release/capture efficiency data more scattered. Nevertheless, we anticipate that these errors have minimal impact on the experiment's conclusions.

the crossover of oxidized Fc1N112-TFSI through the Nafion membrane, which may chemically oxidize the adduct. This highlights the necessity of future electrolyte and electrochemical cell optimizations for practical implementations of EMCC 36 . Nonetheless, the Coulombic efficiency does not display obvious decay over repeated cycling, underlining the robustness of the sorbent itself.

In another set of experiments, we tested the performance of AzPy at a higher percentage of CO_2 removal by decreasing the gas flow rate and increasing the current density (Supplementary Fig. 16). With a feed of 20% CO_2 , the steady-state CO_2 concentration at the sorbent tank outlet is ~3%, corresponding to an 85% reduction in CO_2 partial pressure. Under these conditions, the average capacity utilization efficiency (95%) and release/capture efficiency (85%) remain high. We also demonstrated CO_2 separation with the other families of sp^2 nitrogen moieties discussed in this work (Supplementary Figs. 17–19), which all showed decent performances.

The robustness of AzPy was further demonstrated against O₂ impurity³⁷. Figure 6 is an extension of the experiment in Fig. 5, with 18.5% CO₂ and 3% O₂ as the feed gases. As aforementioned, AzPy possesses a redox potential above the oxygen reduction potential to restrict parasitic reactions with O2. Correspondingly, the system maintains stability over repeated capture-release cycles, with a near-unity capacity utilization efficiency. The average release/capture and Coulombic efficiencies are 97 and 87%, respectively. By integrating the voltage-capacity curve $(Fig.\,6d), the\,electrical\,energy\,consumption\,under\,simulated\,flue\,gas$ was calculated as 120 kJ mol⁻¹ CO₂, which is ~2.5 times the theoretical value (500 mV voltage gap when using Na⁺ as the supporting cation, as shown in Fig. 4e). Currently, the energetics is primarily limited by the low ionic conductivity of the commercial Nafion membrane in organic electrolytes³⁶, which we aim to address in the future via better materials design. A comparison between different EMCC approaches is provided as Supplementary Table 9.

We also performed capture–release cycling under a higher O_2 concentration (15% CO_2 + 5% O_2) with a much greater degree of CO_2 removal (-80%; Supplementary Fig. 20). We observed a slight decrease in the capacity utilization efficiency (86% on average) because of the higher O_2 concentration and the longer contact/reaction time between the reduced sorbent and O_2 . Nevertheless, AzPy still showed a pronounced improvement in separation performance compared with that reported recently with quinone chemistry²³, in which the capacity utilization hovered around only 40% under a mixed gas of 15% CO_2 and 5% O_2 , despite the much lower percentage of CO_2 removal. The effect of water is discussed in Supplementary Note 4 with data shown in Supplementary Fig. 21.

Finally, it is essential to note that continuous CO_2 capture and release with a dual-cell setup similar to the one described in our previous work²³, as opposed to the proof-of-concept batch-based cycling employed here, should be expected for practical implementations. Since the electrochemical sorbent activation is decoupled from CO_2 capture in continuous-flow EMCC, in an actual process, the relative rates of CO_2 uptake by the reduced sorbent, the oxidation of the reduced sorbent by O_2 and the flow of adduct to the desorption cell control the efficiency of the capture–release cycles.

Conclusion

In this work, we report a chemical library of redox-tunable Lewis bases featuring sp^2 nitrogen centres, which can reversibly capture and release CO₂ via an electrochemical reduction and oxidation cycle. With the aid of electrochemical analysis and DFT calculations, the step-by-step mechanism of the CO₂ separation process has been thoroughly investigated. The chemistries reported here create the basis for rational materials design and electrolyte engineering, therefore providing opportunities for property customizations such as the redox potential, CO₂ binding energy, sorbent solubility, nano/microstructures and so on. Importantly, we discovered that the introduction of multifunctionalities to sorbent molecules through extended conjugations can serve as an effective strategy to enhance the selectivity and efficiency of the CO₂ separation process. This concept has been validated successfully using AzPy in a flow carbon capture system under simulated flue gas conditions. Overall, this work provides synthetic and mechanistic guidance for designing redox-tunable CO₂ sorbents.

Methods

Materials

Unless otherwise stated, all of the chemicals were purchased from commercial sources and used without further purification.

Synthesis of 2,7-bis(trifluoromethyl)phenazine

2,7-Bis(trifluoromethyl)phenazine was synthesized following a procedure published previously 38 , by reacting 2-bromo-4-(trifluoromethyl) aniline (1 equiv.) in toluene (0.1 M) with added caesium carbonate (2.0 equiv.), SPhos ligand (0.08 equiv.) and palladium(II) acetate (0.05 equiv.) at 120 °C. The reaction was monitored by thin-layer chromatography. The crude product was purified by column chromatography. 1 H NMR (400 MHz; CDCl₃): δ = 8.63 (s, 2H), 8.43 (d, J = 9.1 Hz, 2H) or 8.04 (d, J = 8.8 Hz, 2H).

Synthesis of 2,2'-AzPy

2,2'-AzPy was synthesized from a modified procedure according to a previous report³⁹. To a solution of 2-aminopyridine (2.5 g; 26.6 mmol) in H₂O (100 ml) was added 8% sodium hypochlorite (aq.; 200 ml) slowly at 0 °C. The mixture was stirred at 0 °C and monitored by thin-layer chromatography. After 2 h, the mixture was filtered. The aqueous filtrate was then extracted with ethyl acetate and the organic layers were combined, dried over MgSO₄ and dried in vacuo. The crude product was purified by column chromatography (ethyl acetate) to give a red crystalline solid (0.58 g; 24%). 1 H NMR (400 MHz; DMSO): δ = 8.78 (d,

J = 3.8 Hz, 2H), 8.11 (td, J = 7.8, 1.5 Hz, 2H), 7.79 (d, J = 8.0 Hz, 2H) or 7.65 (dd, J = 7.2, 4.9 Hz, 2H). ¹³C NMR (101 MHz; DMSO): δ = 162.57, 149.59, 139.15. 126.55 or 113.71.

Synthesis of Fc1N112-TFSI

Fc1N112-TFSI was synthesized according to a previous report via nucleophilic substitution of dimethylaminomethyl ferrocene with bromoethane in acetonitrile, followed by ion exchange of bromide with bis(trifluoromethanesulfonyl)imide in deionized water³⁴.

Electrochemical measurements

Electrochemical measurements were conducted using a BioLogic VSP potentiostat (BioLogic Science Instruments). For the cyclic voltammetry measurements, glassy carbon (\emptyset = 3 mm) was used as the working electrode, platinum wire was used as the counter electrode, silver wire was used as a pseudo-reference electrode and ferrocene was used as an internal reference. In a standard cyclic voltammetry measurement, the molecule of interest was dissolved in DMSO (water < 100 ppm by Karl Fischer titration) at a concentration of 10 mM with 100 mM TBAPF₆ as the supporting salt. Typical cyclic voltammograms were collected at a scan rate of 50 mV s⁻¹. To study the effects of cationic species on the redox behaviour of the sorbent molecules, LiTFSI or sodium bis(trifluoromethanesulfonyl)imide (NaTFSI) was used as the supporting salt.

Bulk electrolysis

Constant current bulk electrolysis of AzPy was carried out to obtain the complete two-electron reduced AzPy(2–) for FTIR studies. The setup consisted of a round-bottom flask with three necks for the working, counter and reference electrodes, respectively. A piece of carbon felt (CT GF030; Fuel Cell Store) was used as the working electrode and a silver wire was used as the reference electrode. The counter electrode was separated from the AzPy solution with a fritted electrode chamber (MR-1196; Bioanalytical Systems). A piece of carbon felt was used as the counter electrode, which was immersed in a neat electrolyte without AzPy. The counter electrode was oxidizing the electrolyte to balance the charge during bulk electrolysis. The three necks were sealed with rubber septa. The solution was magnetically stirred and bubbled with CO₂ or N₂ during bulk electrolysis.

Nafion membrane pretreatment

The Nafion membranes (Nafion 212; Chemours) were pretreated by first boiling the membrane in 3% hydrogen peroxide for 1 h. The membranes were then boiled in 0.25 M sulfuric acid solution for 1 h and cleaned in boiling deionized water for 30 min (twice). Subsequently, the membranes were boiled in 0.25 M sodium hydroxide solution for 1 h and cleaned in boiling deionized water for 30 min (twice). Finally, the membranes were dried under vacuum at 80 °C for at least 2 d and stored in DMSO containing 0.25 M NaTFSI.

EMCC flow cell setup

In a typical experiment, the sorbent tank (20 ml scintillation vial with septum cap) was continuously bubbled with CO_2 feed gas (balanced by N_2) with the flow rate controlled by a mass flow controller (Cole-Parmer). For testing under simulated flue gas conditions, a gas mixture of either 18.5% $CO_2 + 3\%$ O_2 or 15% $CO_2 + 5\%$ O_2 balanced by N_2 was used. An infrared-based CO_2 sensor (SprintIR-W 100%) was connected at the gas exit to monitor the CO_2 concentration continuously. The tank headspace was filled with plastic beads (McMaster-Carr) to limit the mixing time in the headspace. The Fc1N112-TFSI tank was kept air free. A two-channel peristaltic pump (Ismatec Reglo ICC Digital Pump; Cole-Parmer) pumped the sorbent and the Fc1N112-TFSI electrolyte to a commercial flow cell (Scribner) at a flow rate of 3 ml min $^{-1}$. The flow cell utilized graphite plates with 5 cm 2 interdigitated flow fields pressed against carbon felt electrodes (CT GF030; Fuel Cell

Store) to distribute the liquid flow. A Nafion 212 membrane was placed between the two carbon felt electrodes. The carbon felt was held in place by 3-mm-thick PTFE frames and the cell was kept sealed by Kalrez fluoropolymer elastomer gaskets (0.02 inches thick). $\rm CO_2$ capture was carried out in a constant current mode while the release was carried out following a constant current/constant voltage protocol (that is, oxidizing the adduct at a constant current until a specific cut-off voltage followed by a constant voltage hold (the cut-off current for the constant voltage hold was 10% of the value used in the constant current oxidation). Additional experimental details of the flow system are included alongside images in the Supplementary Information and the cycling protocols of each experiment are provided in the corresponding figure captions.

DFT calculations

The Gaussian $16 \operatorname{code}^{40}$ was used in the DFT calculations with the B3LYP functional 41,42 and the $6 \cdot 31 + + \operatorname{G}(d,p)$ basis set $^{43-45}$. The conductor-like polarizable continuum model was used to simulate the solvation effect of DMSO solvent at room temperature 46 . To simulate the processes in a solvated environment, free energies excluding translational contributions at 298 K were calculated. A benchmark of the calculated redox potentials against the experimentally measured potentials can be found in Supplementary Fig. 2. A comparison of functionals can be found in Supplementary Table 2. FTIR vibrational frequencies were calculated for optimized structures by determining the second derivative of the energy with respect to the nuclear coordinates and then transforming to mass-weighted coordinates.

Data availability

The data generated or analysed during this study are included in the published article and its Supplementary Information file. Source data are provided with this paper.

References

- IPCC Special Report on Global Warming of 1.5 °C (eds Masson-Delmotte, V. et al.) (WMO, 2018).
- Chu, S. Carbon capture and sequestration. Science 325, 1599 (2009).
- 3. Haszeldine, R. S. Carbon capture and storage: how green can black be? *Science* **325**, 1647–1652 (2009).
- 4. Bui, M. et al. Carbon capture and storage (CCS): the way forward. Energy Environ. Sci. 11, 1062–1176 (2018).
- Shi, X. et al. Sorbents for the direct capture of CO₂ from ambient air. Angew. Chem. Int. Ed. 59, 6984–7006 (2020).
- Sanz-Pérez, E. S., Murdock, C. R., Didas, S. A. & Jones, C. W. Direct capture of CO₂ from ambient air. Chem. Rev. 116, 11840–11876 (2016).
- Rochelle, G. T. Amine scrubbing for CO₂ capture. Science 325, 1652–1654 (2009).
- Said, R. B., Kolle, J. M., Essalah, K., Tangour, B. & Sayari, A. A unified approach to CO₂-amine reaction mechanisms. ACS Omega 5, 26125–26133 (2020).
- Davis, J. & Rochelle, G. Thermal degradation of monoethanolamine at stripper conditions. *Energy Procedia* 1, 327–333 (2009).
- Rochelle, G. T. in Absorption-Based Post-combustion Capture of Carbon Dioxide 35–67 (Woodhead Publishing, 2016).
- Vasudevan, S. et al. Energy penalty estimates for CO₂ capture: comparison between fuel types and capture-combustion modes. *Energy* 103, 709–714 (2016).
- Zheng, R. F. et al. A single-component water-lean post-combustion CO₂ capture solvent with exceptionally low operational heat and total costs of capture—comprehensive experimental and theoretical evaluation. *Energy Environ. Sci.* 13, 4106–4113 (2020).

- McDonald, T. M. et al. Cooperative insertion of CO₂ in diamine-appended metal-organic frameworks. *Nature* 519, 303–308 (2015).
- Park, Y., Lin, K.-Y. A., Park, A.-H. A. & Petit, C. Recent advances in anhydrous solvents for CO₂ capture: ionic liquids, switchable solvents, and nanoparticle organic hybrid materials. Front. Energy Res. 3, 42 (2015).
- Halliday, C. & Hatton, T. A. Sorbents for the capture of CO₂ and other acid gases: a review. *Ind. Eng. Chem. Res.* 60, 9313–9346 (2021).
- Rheinhardt, J. H., Singh, P., Tarakeshwar, P. & Buttry, D. A. Electrochemical capture and release of carbon dioxide. ACS Energy Lett. 2, 454–461 (2017).
- Renfrew, S. E., Starr, D. E. & Strasser, P. Electrochemical approaches toward CO₂ capture and concentration. ACS Catal. 10, 13058–13074 (2020).
- 18. Sharifian, R., Wagterveld, R. M., Digdaya, I. A., Xiang, C. & Vermaas, D. A. Electrochemical carbon dioxide capture to close the carbon cycle. *Energy Environ*. Sci. **14**, 781–814 (2021).
- Stern, M. C., Simeon, F., Herzog, H. & Hatton, T. A. Post-combustion carbon dioxide capture using electrochemically mediated amine regeneration. *Energy Environ. Sci.* 6, 2505–2517 (2013).
- Voskian, S. & Hatton, T. A. Faradaic electro-swing reactive adsorption for CO₂ capture. *Energy Environ. Sci.* 12, 3530–3547 (2019).
- 21. Liu, Y. et al. Electrochemically mediated gating membrane with dynamically controllable gas transport. *Sci. Adv.* **6**, eabc1741 (2020).
- 22. Liu, Y., Ye, H.-Z., Diederichsen, K. M., Van Voorhis, T. & Hatton, T. A. Electrochemically mediated carbon dioxide separation with quinone chemistry in salt-concentrated aqueous media. *Nat. Commun.* 11, 2278 (2020).
- Diederichsen, K. M., Liu, Y., Ozbek, N., Seo, H. & Hatton, T.
 A. Toward solvent-free continuous-flow electrochemically mediated carbon capture with high-concentration liquid quinone chemistry. *Joule* 6, 221–239 (2022).
- 24. Seo, H., Rahimi, M. & Hatton, T. A. Electrochemical carbon dioxide capture and release with a redox-active amine. *J. Am. Chem. Soc.* **144**, 2164–2170 (2022).
- 25. Mizen, M. B. & Wrighton, M. S. Reductive addition of CO_2 to 9,10-phenanthrenequinone. *J. Electrochem. Soc.* **136**, 941–946 (1989).
- Scovazzo, P., Poshusta, J., DuBois, D., Koval, C. & Noble, R. Electrochemical separation and concentration of <1% carbon dioxide from nitrogen. *J. Electrochem. Soc.* 150, D91 (2003).
- Simpson, T. C. & Durand, R. R. Reactivity of carbon dioxide with quinones. *Electrochim. Acta* 35, 1399–1403 (1990).
- Simeon, F. et al. Electrochemical and molecular assessment of quinones as CO₂-binding redox molecules for carbon capture. J. Phys. Chem. C 126, 1389–1399 (2022).
- 29. Singh, P. et al. Electrochemical capture and release of carbon dioxide using a disulfide–thiocarbonate redox cycle. *J. Am. Chem.* Soc. **139**, 1033–1036 (2017).
- Ranjan, R. et al. Reversible electrochemical trapping of carbon dioxide using 4,4'-bipyridine that does not require thermal activation. J. Phys. Chem. Lett. 6, 4943–4946 (2015).
- 31. Assary, R. S., Brushett, F. R. & Curtiss, L. A. Reduction potential predictions of some aromatic nitrogen-containing molecules. *RSC Adv.* **4**, 57442–57451 (2014).
- 32. Vasudevan, D. & Wendt, H. Electroreduction of oxygen in aprotic media. *J. Electroanal. Chem.* **392**, 69–74 (1995).
- 33. Zhuang, Z. et al. Spectroscopy of 4,4'-azopyridine by density functional theory and surface-enhanced Raman scattering. *J. Mol. Struct.* **794**, 77–82 (2006).

- Wei, X. et al. Towards high-performance nonaqueous redox flow electrolyte via ionic modification of active species. Adv. Energy Mater. 5, 1400678 (2015).
- Milshtein, J. D. et al. Towards low resistance nonaqueous redox flow batteries. J. Electrochem. Soc. 164, A2487–A2499 (2017).
- Yuan, J. et al. Membranes in non-aqueous redox flow battery: a review. J. Power Sources 500, 229983 (2021).
- IPCC Special Report on Carbon Dioxide Capture and Storage (eds Metz, B. et al.) (Cambridge Univ. Press, 2005).
- Winkler, J. D., Twenter, B. M. & Gendrineau, T. Synthesis of substituted phenazines via palladium-catalyzed aryl ligation. Heterocycles 84, 1345–1353 (2012).
- Fang, W., Liu, X., Lu, Z. & Tu, T. Photoresponsive metallo-hydrogels based on visual discrimination of the positional isomers through selective thixotropic gel collapse. *Chem. Commun.* 50, 3313– 3316 (2014).
- 40. Frisch, M. J. et al. Gaussian 16 Revision C.01 (Gaussian Inc., 2016).
- 41. Becke, A. D. Density-functional thermochemistry. III. The role of exact exchange. *J. Chem. Phys.* **98**, 5648–5652 (1993).
- Lee, C., Yang, W. & Parr, R. G. Development of the Colle–Salvetti correlation-energy formula into a functional of the electron density. *Phys. Rev. B* 37, 785–789 (1988).
- Clark, T., Chandrasekhar, J., Spitznagel, G. W. & Schleyer, P. V.
 R. Efficient diffuse function-augmented basis sets for anion calculations. III. The 3-21+G basis set for first-row elements, Li–F. J. Comput. Chem. 4, 294–301 (1983).
- 44. Hariharan, P. C. & Pople, J. A. The influence of polarization functions on molecular orbital hydrogenation energies. *Theor. Chim. Acta* **28**, 213–222 (1973).
- 45. Hehre, W. J., Ditchfield, R. & Pople, J. A. Self-consistent molecular orbital methods. XII. Further extensions of gaussian-type basis sets for use in molecular orbital studies of organic molecules. *J. Chem. Phys.* **56**, 2257–2261 (1972).
- Barone, V. & Cossi, M. Quantum calculation of molecular energies and energy gradients in solution by a conductor solvent model. J. Phys. Chem. A 102, 1995–2001 (1998).

Acknowledgements

Yayuan Liu. and T.A.H. acknowledge support from the National Science Foundation (grant number 2029442). Yayuan Liu and X.L. acknowledge support from the Johns Hopkins University and American Chemical Society Petroleum Research Fund (65626-DNI4). Yuanyue Liu acknowledges support from the National Science Foundation (grant numbers 1900039 and 2029442), American Chemical Society

Petroleum Research Fund (60934-DNI6) and Welch Foundation (grant number F-1959-20210327). For the calculations, we used computational resources at the Extreme Science and Engineering Discovery Environment, Texas Advanced Computing Center, Argonne National Laboratory and Brookhaven National Laboratory. We thank K. M. Diederichsen, H. Seo and E. Wenbo Zhao for helpful discussions.

Author contributions

Yayuan Liu conceived of the project and designed the experiments. Yayuan Liu and X.L. carried out the experiments and analysed the data. X.Z. performed the DFT calculations. Yayuan Liu, Yuanyue Liu and T.A.H. supervised the project. Yayuan Liu, X.L. and X.Z. wrote the paper. All authors discussed the results and revised or commented on the manuscript.

Competing interests

The authors declare no competing interests.

Additional information

Supplementary information The online version contains supplementary material available at https://doi.org/10.1038/s41560-022-01137-z.

Correspondence and requests for materials should be addressed to Yuanyue Liu, T. Alan Hatton or Yayuan Liu.

Peer review information *Nature Energy* thanks Rajeev Assary and the other, anonymous, reviewer(s) for their contribution to the peer review of this work.

Reprints and permissions information is available at www.nature.com/reprints.

Publisher's note Springer Nature remains neutral with regard to jurisdictional claims in published maps and institutional affiliations.

Springer Nature or its licensor holds exclusive rights to this article under a publishing agreement with the author(s) or other rightsholder(s); author self-archiving of the accepted manuscript version of this article is solely governed by the terms of such publishing agreement and applicable law.

© The Author(s), under exclusive licence to Springer Nature Limited 2022